Chapter 10

First analysis using the Haser model

Parallel to the data reduction a first analysis using the Haser model was done. The determination of production rates and Haser scale lengths for CN, C_2, C_3 and NH_2 has been done as a contribution to the paper by Rauer *et al.* [2002]. During this work it became obvious that the formation of C_2 and C_3 can not be explained using a simple Haser model. This was the starting point for the main part of this work described in chapter V.

10.1 Haser model

A model often used to derive gas production rates is the Haser model [Haser and Swings, 1957]. This rather simple model is based on a number of assumptions. Outgassing is assumed to be isotropic and the gas streams of the nucleus with a constant radial velocity. Parent species coming off the nucleus are decaying directly to the observed daughter-species, which in turn decay to a granddaughter species. Using these assumptions the number of particles n in a given distance from the nucleus ρ can be derived by

$$n(\rho) = \frac{Q}{4\pi v \rho^2}\left(\frac{l_d}{l_p - l_d}\right)\left(e^{-\frac{\rho_n}{l_p}} - e^{-\frac{\rho_n}{l_d}}\right) \tag{10.1}$$

ρ	nucleocentric distance
$\rho_n = \rho - r_n$	reduced nucleocentric distance (r_n radius of the nucleus)
l_p, l_d	scale lengths for parent and daughter species
Q	production rate
v	gas velocity

In the most simple case, where the observed daughter species is produced in a single step from a parent species which sublimes of the nucleus and expands at constant speed, the scale lengths used in formula (10.1) can be written as

$$l = \tau \cdot v \tag{10.2}$$

where τ is the life time against destruction. The main destruction process in the coma is photodissociation.
The real processes in the coma are usually more complex. Some of the observed daughter species are not produced in a single-step process from a single parent molecule. A daughter molecule can have different parent molecules and it can be produced by a number of different reaction pathways. There might also be a number of intermediate steps instead of a single production step, so that instead of a daughter-species a grand- or even a grand-grand-daughter species is observed. Furthermore if the destruction process is exothermic the excess energy is imparted on the reaction products. This usually leads to an increased velocity of the lighter fragments.
For these reasons it is more appropriate to view l_p and l_d as 'effective' scale lengths. Only in the most simple case it is possible to give a physical interpretation for the Haser scale lengths.
Column densities can be derived by an integration along the line of sight of equation (10.1). These can be compared to the observed spatial distribution of the daughter species in the coma. By variation of the values for Q, l_p and l_d a model profile can be generated which fits best the observations. This method has been used to derive production rates and 'effective' Haser scale lengths in this work.
Effective Haser scale lengths have been determined for a number of molecules using this method and are published in the literature. The rapidly diminishing brightness of most comets allows to determine scale lengths with the above mentioned method only at heliocentric distances less than 2 AU. It is necessary to extrapolate the scale lengths for comets at larger heliocentric distances. Later in this work it will be shown, that comet Hale-Bopp allowed for the first time to determine scale lengths directly for larger heliocentric distances. The differences between the extrapolation and the direct determined values will be discussed. Some values from the literature given in the form $l_{p/d}(r_h) = l_{p/d} \cdot r_h^b$ are listed in Table 10.1.
The Haser model is only a very crude approximation of the real physical and chemical processes in the coma of a comet. However, it is widely used, due to the fact that production rates can be derived very easily using scale lengths published in the literature. This allows to easily compare different observations and thus the Haser model is used as a sort of reference.

10.2 Numerical approach

Haser scale lengths have been derived from the measured spatial column density profiles of the daughter radicals. This was done by finding the best fit of column density profiles computed by integration of equation (10.1) to the measured column density profiles.
The Haser model yields number densities n(ρ) (green lines in figure 10.1), where ρ is the nucleocentric distance. An observer from the Earth measures a column density $N(\rho^*) = \int n(\rho)$, where ρ^* (marked by the green dots in figure 10.1) is the projected nucleocentric distance on the sky plane. An outside observer looking at the coma sees at a given nucleocentric distance the light emitted by all molecules along a line through the coma, the line of sight (the blue lines in figure 10.1). To convert from number densities as calculated by the Haser model

Molecule	parent		daughter	
A'Hearn *et al.* [1995]				
	$l_p[km]$	b	$l_d[km]$	b
CN	$1.3\ 10^4$	2	$2.2\ 10^5$	2
C_2	$2.2\ 10^4$	2	$6.6\ 10^4$	2
C_3	$2.8\ 10^3$	2	$2.7\ 10^4$	2
Fink *et al.* [1991]				
CN	$2.8\pm1.4\ 10^4$	2	$3.2\ 10^5$	2
C_2	$5.8\pm0.5\ 10^4$	2	$5.8\pm0.5\ 10^4$	2
NH_2	$4.9\pm1.5\ 10^3$	2	$6.2\pm2.0\ 10^3$	2
Cochran [1985]; Cochran *et al.* [1992]				
CN	$1.4\ 10^4$	2	$3.0\ 10^5$	2
C_2	$2.5\ 10^4$	2.5	$1.2\ 10^5$	2
C_3	$3.1\ 10^3$	2	$1.5\ 10^5$	2
NH_2	$4.1\ 10^3$	2	$6.2\ 10^4$	2

Table 10.1: Scale lengths for parent and daughter species as given in the literature

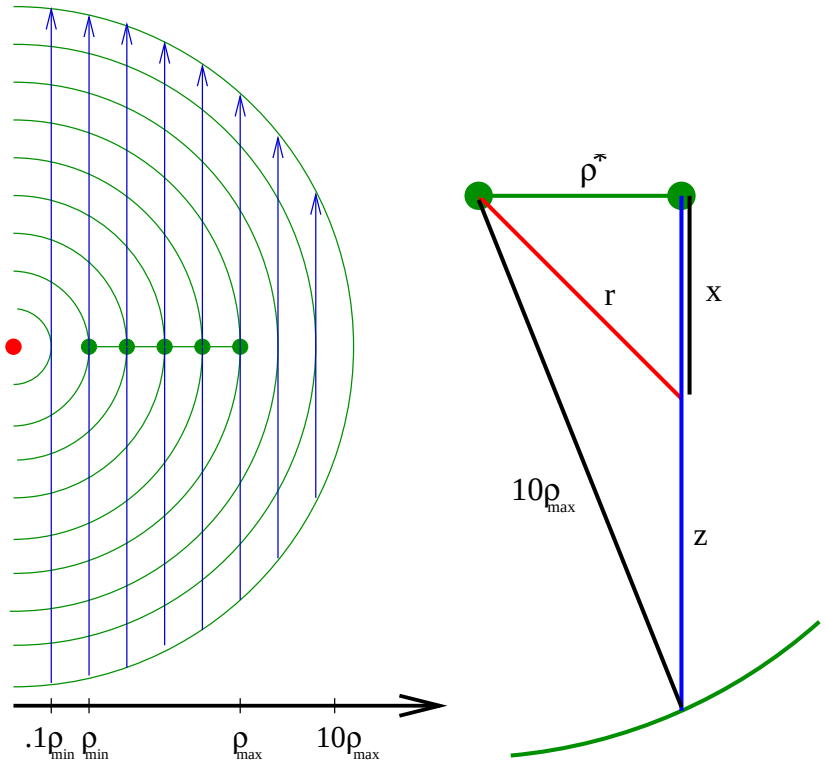

Figure 10.1: Line of sight integration used for the Haser model

to column densities as observed from Earth, an integration along the line of sight (LOS) is performed. There are two approaches to obtain column densities from the Haser model,

an analytical and a numerical one. For the analytic approach equation (10.1) is integrated yielding Bessel functions. The integration is performed along the LOS.
For this work the numerical approach was used. The numerical accuracy achievable in IDL was higher than using the analytical approach. Using equation (10.1) the number densities have been computed for a nucleocentric distance range from $0.1 \cdot \rho_{\min}$ to $10 \cdot \rho_{\max}$, where $\rho_{\min}$ and $\rho_{\max}$ are the minimum and maximum of the nucleocentric distance range covered in the observation. Extending the nucleocentric distance range by a factor of 10 is sufficient to get a baseline long enough for the LOS integration of the outermost points of the observed spatial profiles. Tests for several heliocentric distances have shown that an extension by a factor of 5 is already sufficient, the additional factor 2 gives a safety margin for future use of the integration routine.
The maximum coma extension along the LOS for a given projected nucleocentric distance ρ^* is defined by $z = \sqrt{10 \cdot \rho_{\max} - \rho^*}$ (see right part of figure 10.1). This sets the integration limits and the column density $N(\rho^*)$ is given by

$$N(\rho^*) = \int_{-z}^{z} \frac{Q}{4\pi v r_n^2} \left(\frac{l_d}{l_p - l_d}\right)\left(e^{(} - \frac{r(x)}{l_p}\right) - e\left(-\frac{r(x)}{l_d}\right)\Big) d^z \tag{10.3}$$

ρ^*	projected nucleocentric distance
r_n	Radius of the nucleus
$r(x)$	$r(x) = \sqrt{\rho^{*2} + x^2}$ nucleocentric distance (see right of figure 10.1)
l_p, l_d	scale-lengths for parent- and daughter-species
Q	production rate
v	gas velocity

The numerical integration is performed using the Romberg integration method ([Stoer and Bulirsch, 1980] and [Press *et al.*, 1992]). The line of sight is divided in 10000 equi-distant steps for the integration. This number is again the result of extensive testing. For more than 5000 steps the result of the integration does not show significant changes. As before an additional factor of 2 has been added as a safety margin for future use of the integration procedure.
The radius of the nucleus r_n is set to 25 km (see Altenhoff *et al.* [1999]). For the gas velocity v the empirically determined evolution with heliocentric distance $v = 1.112 \cdot r_h^{-0.41} \frac{\mathrm{km}}{\mathrm{s}}$ was adopted [Biver *et al.*, 1997].
In equation (10.3) three unknowns are left on the right side, namely the production rate Q and the parent and daughter scale lengths l_p and l_d. The value on the left side of the equation corresponds to the spatial column density profiles obtained from the measurements.
The scale lengths for the parent and daughter molecules of the observed species have been determined by a number of authors for different comets. Some values are given in Table 10.3. Using a power law with the parameters given in the table, these values can be extrapolated to the heliocentric distances of the Hale-Bopp observations studied in this work. This eliminates two of the three unknown quantities and allows to determine the production rate Q.

Heliocentric distance [AU] [AU]	**Species**	**Three parameter fit** Deviation [%]	**l_d fixed on smallest value** Deviation [%]
3.78	CN	3.1	2.9
	C_2	9.1	8.8
	C_3	10.4	9.5
	NH_2	14.7	11.2
4.14	CN	3.1	2.3
	C_2	8.3	6.3
	C_3	9.7	7.4
	NH_2	13.4	11.1
4.74	CN	0.5	1.1
	C_2	3.0	2.3
	C_3	5.8	4.1
	NH_2	7.9	7.1

Table 10.2: Error in determination of Haser parent scale

The basic principle to determine the unknown quantities is an one or three parameter fit using a forward calculation approach. The best match to the profiles is found using a Levenberg-Marquardt least-squares fit routine in IDL, adopted from Numerical Recipes [Press *et al.*, 1992].

This technique would in principle allow to determine production rates and scale lengths of parent and daughter species for each observed species from each spatial profile. Testing this method in practice has shown that it is in most cases impossible to determine the scale length of the daughter species from the observations used here. In these cases the fitting procedure returns unrealistically large values for the daughter scale lengths, generally several magnitudes larger than the slit lengths. However, this is not a numerical issue but has a physical reasoning. All observations were obtained at large heliocentric distances. The projected nucleocentric distance accessible to the observation is limited by the slit length. The projection of the slit length on the sky scales directly with the heliocentric distance. The Haser scale lengths scale in general with the square of the heliocentric distance. For the following it is assumed that the chemistry within the field of view is dominated by the destruction of the parent molecule. The daughter species are mainly destroyed at nucleocentric distances which are not covered in the observed spatial profiles. For this reason the daughter scale lengths can not be constraint from the observations.

For the fitting procedure the daughter scale length was kept fixed at a large value (in numbers: it was set to infinity which translates in IDL to `!values.f_infinity`) assuming that all destruction of the daughter molecules occurs far outside the FOV. The assumption was tested by running the fit procedure three times, once determining only the parent scale lengths, while setting the daughter scale lengths to infinity, the second time determining parent and daughter scale lengths and the third time determining the parent scale lengths while setting the daughter scale lengths to the smallest value published in the literature

(see Table 10.1. For the second and third case the deviation of the resulting Haser parent scale lengths relative to the first case is shown in Table 10.2 for a subset of the observations covering the whole range of heliocentric distances. The deviation is always smaller than 15%. There is no indication of a tendency to produce always larger or always smaller parent scale lengths. The most prominent differences occur for NH_2, which has a relative small daughter scale length. The deviation decreases with increasing heliocentric distance as expected. However this effect is small and is included in the error given for the parent scale lengths and the power law for the evolution with heliocentric distance.

10.3 Determination of Haser scale lengths

Using the method described above Haser parent scale lengths have been determined for the whole data set. For each night the mean profiles of each species (as described in section 8) has been used. As starting values for the fitting procedure published Haser parent scale lengths (see table 10.3) have been used. For CN, as an example these results in 3 separate runs of the fitting routine, starting with the Haser parent scale lengths provided by A'Hearn *et al.* [1995], Cochran *et al.* [1992] and Fink *et al.* [1991]. This number was doubled by fitting both spatial directions separately. The convergence of the separate runs was used as a test for the data quality. The scatter of the results is always smaller than 5%. There are also no significant differences between the spatial directions. For this reason the resulting parent scale lengths was determined as the mean of the separate fits, the errors were calculated using the least mean square errors of the separate fits. Figure 10.2 is a plot of the Haser parent scale lengths versus heliocentric distance. For the weak NH_2 emission it was possible to determine reliable parent scale lengths only up to 3.78 AU. For larger heliocentric distances the fits for the Haser scale lengths did not converge, because of too large scatter in the data points.
To study the evolution of Haser parent scale lengths with heliocentric distance, a simple power law of the type

$$l = l_p \cdot r_h^{b_p} \tag{10.4}$$

has been fitted to the data. The parameter l_p and b_p have been determined by a linear fit to the double logarithmic plot of the scale lengths versus heliocentric distance (see Figure 10.2). The resulting values are given in Table 10.3 in comparison to the literature.
Haser scale lengths derived in this work using the power law given above are strictly valid only in the range $r_h \geq 3$ AU. Similiarly, the values published in the literature are strictly valid only for the heliocentric distance range used to determine them, generally smaller than 2 AU.
One has to be cautious in comparing the values for the parent Haser scale length l_p as given in Table 10.3 derived in this work with the values given in the literature. Based on the power law fit l_p is the parent Haser scale length at 1 AU heliocentric distance. However, this is based on the assumption that the evolution with heliocentric distance does not change from 1 to 3 AU. This assumption can not be proven based on the data used in this work.

Molecule	$\mathbf{l}_p$ **[km]**	b_p	$\mathbf{l}_d$ **[km]**	b_d	**Reference**
CN	**5.4±1.4 10^4**	**1.3±0.2**	-	-	**Rauer *et al.* [2002]**
	1.3 10^4	2	2.2 10^5	2	A'Hearn *et al.* [1995]
	2.8±1.4 10^4	2	3.2 10^5	2	Fink *et al.* [1991]
	1.4 10^4	2	3.0 10^5	2	Cochran *et al.* [1992]
$\mathbf{C_2}$	**1.6±0.8 10^4**	**2.8±0.4**	-	-	**Rauer *et al.* [2002]**
	2.2 10^4	2	6.6 10^4	2	A'Hearn *et al.* [1995]
	5.8±0.5 10^4	2	5.8±0.5 10^4	2	Fink *et al.* [1991]
	2.5 10^4	2.5	12.0 10^4	2	Cochran *et al.* [1992]
$\mathbf{C_3}$	**1.3±0.4 10^3**	**2.6±0.2**	-	-	**Rauer *et al.* [2002]**
	2.8 10^3	2	2.7 10^4	2	A'Hearn *et al.* [1995]
	3.1 10^3	2	15.0 10^4	2	Cochran *et al.* [1992]
$\mathbf{NH_2}$	**9.5±11.1 10^3**	**1.5±0.9**	-	-	**Rauer *et al.* [2002]**
	4.9±1.5 10^3	2	6.9±2.0 10^3	2	Fink *et al.* [1991]
	4.1 10^3	2	62.0 10^3	2	Cochran *et al.* [1992]

Table 10.3: Parent and daughter Haser scale lengths, l_p and l_d, published in the literature and derived in this work. The scale lengths can be scaled to other heliocentric distances as $\mathrm{l}_{p,d} \cdot \mathrm{r}_h^{b_{p,d}}$ (see equation (10.4)) [Rauer *et al.*, 2002].

It is interesting to take a closer look at the exponent b in equation (10.4) giving the evolution with heliocentric distance. According to equation (10.2) in section 10.1 the Haser parent scale length is defined as $l_p = \tau_p \cdot v$ where τ_p is the lifetime of the parent species and v is the velocity of the gas. The lifetime scales with the heliocentric distance as r_h^2. For the gas velocity the empirical expression $v = 1.112 \cdot r_h^{-0.41} \frac{\mathrm{km}}{\mathrm{s}}$ by Biver *et al.* [1997] was used. Therefore, the theoretical dependence of l versus r_h can be (roughly) described as

$$l \sim r_h^2 \cdot r_h^{-0.41} = r_h^{1.59} \tag{10.5}$$

If the daughter species are produced in a single photodissociation reaction as assumed by the Haser model the exponent b in equation (10.4) has to be close to ≈ 1.6. Deviations from this value would be indicative for a different formation process or additional acceleration processes.

For NH_2 the derived scaling factor $b = 1.5 \pm 0.9$ is in good agreement with the expected value. This is a strong indicator for the formation of NH_2 from a single parent species in a single photodissociation step. The dominant N-bearing species in comets is NH_3 [Bird *et al.*, 1997]. Looking at the photochemistry of the possible NH_2 parents (see section 5.4) it is most likely, that in comet Hale-Bopp at heliocentric distances $r_h \geq 3.0$ AU NH_3 is indeed the main source of NH_2. This is in agreement with the results for comet Hyakutake by Kawakita and Watanabe [1998].

For CN the derived scaling factor is $b = 1.3 \pm 0.2$. This is within the uncertainties in agreement with formation of CN by single step photodissociation of HCN. The small deviation from the expected value of $b \approx 1.6$ is explained by the additional excess energy which is

imparted on the CN radical upon photodissociation (see section 5.3). This excess energy leads to an additional acceleration of the observed daughter species, violating the assumption of constant outflow velocity made by the Haser model. See Rauer *et al.* [2002] for a more detailed discussion.
The values derived for C_2 ($b = 2.8 \pm 0.4$) and C_3 ($b = 2.6 \pm 0.2$) show no agreement with the expected value of $b \approx 1.6$. The value for C_2 is close to the value ($b = 2.5$) derived previously by Cochran *et al.* [1992] (see Table 10.3). They had already proposed a formation of C_2 in a two step photodissociation reaction for C_2H_2 similar to Jackson [1976]. The results obtained in this work clearly indicate that neither C_2 nor C_3 are formed in a single photodissociation process from a single parent molecule. This is in agreement with the complex formation chemistry for plausible C_2 and C_3 parents as presented in section 11.1 and 11.2. To model these processes accordingly clearly a more complex model than the Haser model is needed.

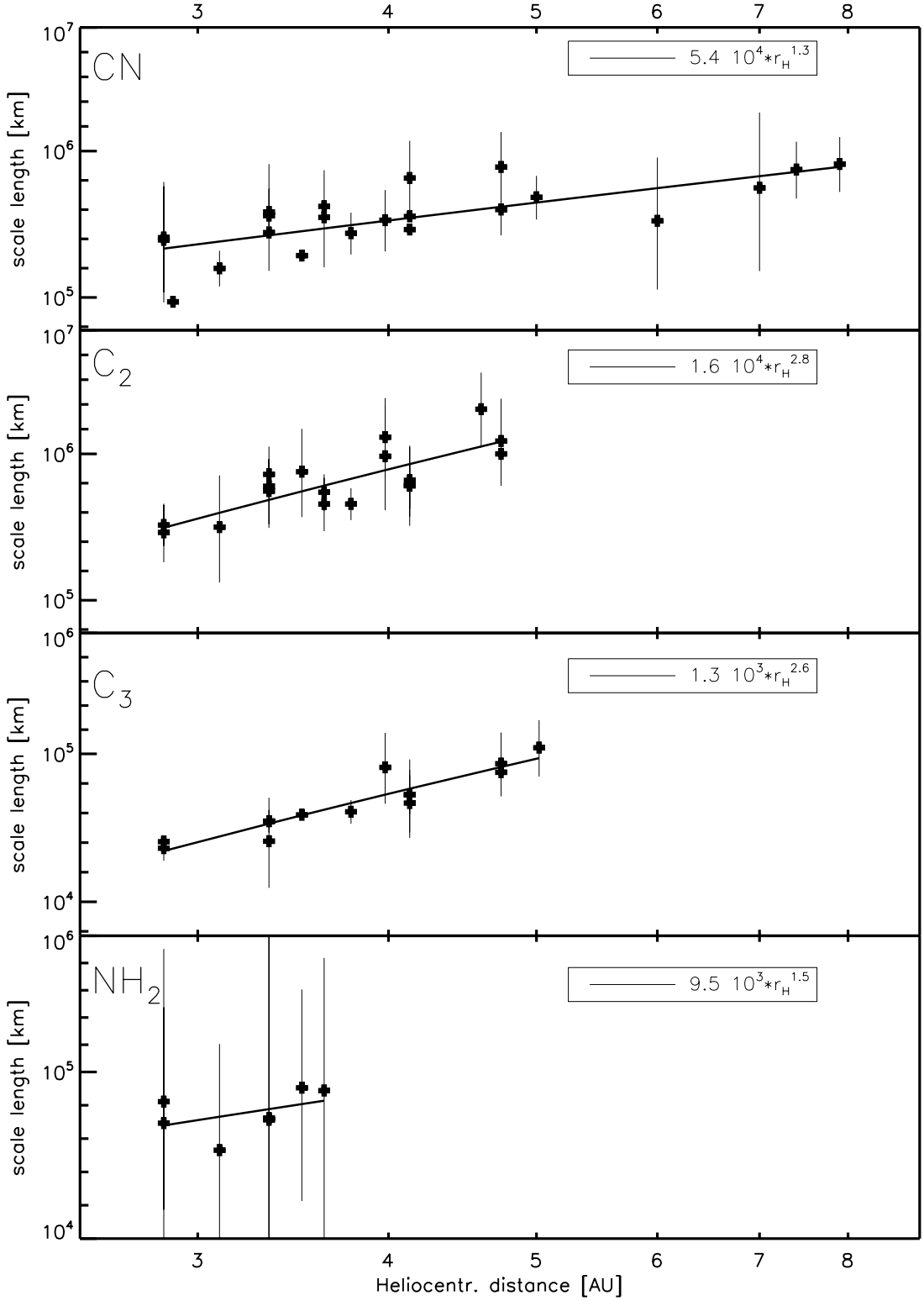

Figure 10.2: Haser parent scale lengths versus heliocentric distance. Solid line: fit of equation (10.4) to the data [Rauer *et al.*, 2002].

10.4 Production rates for all observed radicals

To determine the production rate Q the Haser scale lengths are assumed as fixed values. In this case a fit of equation (10.3) with Q as the only free parameter is performed. The Haser scale lengths have been scaled using the expression $l_{p,d} \cdot r_h^{b_{p,d}}$ for the parent l_p and the daughter l_d scale lengths with the values given in Table 10.3. For the Haser parent scale lengths determined in this work, the corresponding daughter scale lengths have been set to infinity (in numbers it was set to infinity, which translates in IDL to `!values.f_infinity`). It should be pointed out that the scaled Haser parent scale lengths may differ slightly from the directly determined Haser parent scale lengths. As can be seen from the differences between the line representing the fit and the actual data points in figure 10.2 the differences are generally small and within the error bars. The effect on the resulting production rates is less than 10%. Haser parent scale lengths could not be determined for all observations, especially not at large heliocentric distances. Using scaled values (10.4) the resulting production rates Q are comparable over the whole range of heliocentric distances.

Figure 10.3 shows some examples of the fitting process. Displayed are the radial profiles of the column density of CN, C_2, C_3 and NH_2 for four nights. These nights cover the whole range of heliocentric distances observed during the longterm monitoring program where all species could be detected. Overplotted are the profiles obtained from the Haser model as best fit for the different scale lengths. The measured profiles and the fitted Haser profiles of the radicals have been offset vertically for display.

The observations at 3.66 AU (top left panel in figure 10.3) have been obtained at the Danish 1.5m telescope. Clearly visible is the effect of the reflex in the optical system (see section IV) on the C_3 profile. All other observations have been obtained at the ESO 1.52m telescope.

For the CN emission profile the Haser profiles for the different scale lengths show only little differences. However the fits using the scale lengths determined in this work show overall the best match.

For the C_2 emission profile the Haser scale lengths determined in this work show the best fit to the measured profiles. The values given by Cochran (see Table 10.3) result also in good approximations, while the profiles generated using other scale lengths are generally too steep.

For the C_3 emission profile the Haser scale lengths determined in this work and the values given by Cochran *et al.* [1992] (see Table 10.3) show about equally good results, overall better than the results achievable with the values given by A'Hearn *et al.* [1995].

For the NH_2 emission profiles the Haser scale lengths determined in this work show again the best overall match, as expected.

In summary, the determined Haser parent scale lengths show a good agreement over all species and over the whole range of heliocentric distances covered in this work. While only four nights are presented here as example, the fitting procedure generates similar plots for each night and the quality of the fit has been checked for each night separately.

The resulting production rates computed using the Haser scale lengths determined in this work are displayed in Table 10.4. Figure 10.4 is a plot of the production rate Q for all observed species over heliocentric distance. The production rates have been calculated for

all sets of Haser scale lengths given in Table 10.3.
To obtain upper limits on the production rate for a species which could not be clearly detected anymore, the same procedure is used as for determining all other production rates. This guarantees the consistency of the obtained production rates. Instead of the spatial profile of the emission line a 3σ upper limit was computed, by integrating over the wavelength range of the emission. If there is any emission in this wavelength range its signal is weaker than the noise, otherwise it could be identified in the spectrum. Therefore, integrating the noise to obtain a spatial profile will yield a meaningful upper limit for the production rates. Upper limits are indicated by downward pointing arrows in Figure 10.4. In case of the C_3 detection at 7.0 AU, the C_3 emission band could be identified visually (see chapter 7), but integrating the flux was difficult. The area of the spectrum within the nominal wavelength range of the C_3 emission band was integrated. The contaminations within this range, mainly due to residuals of the underlying continuum, are close to the signal. Thus the production rate for C_3 at 7.0 AU can be interpreted only as an upper limit.

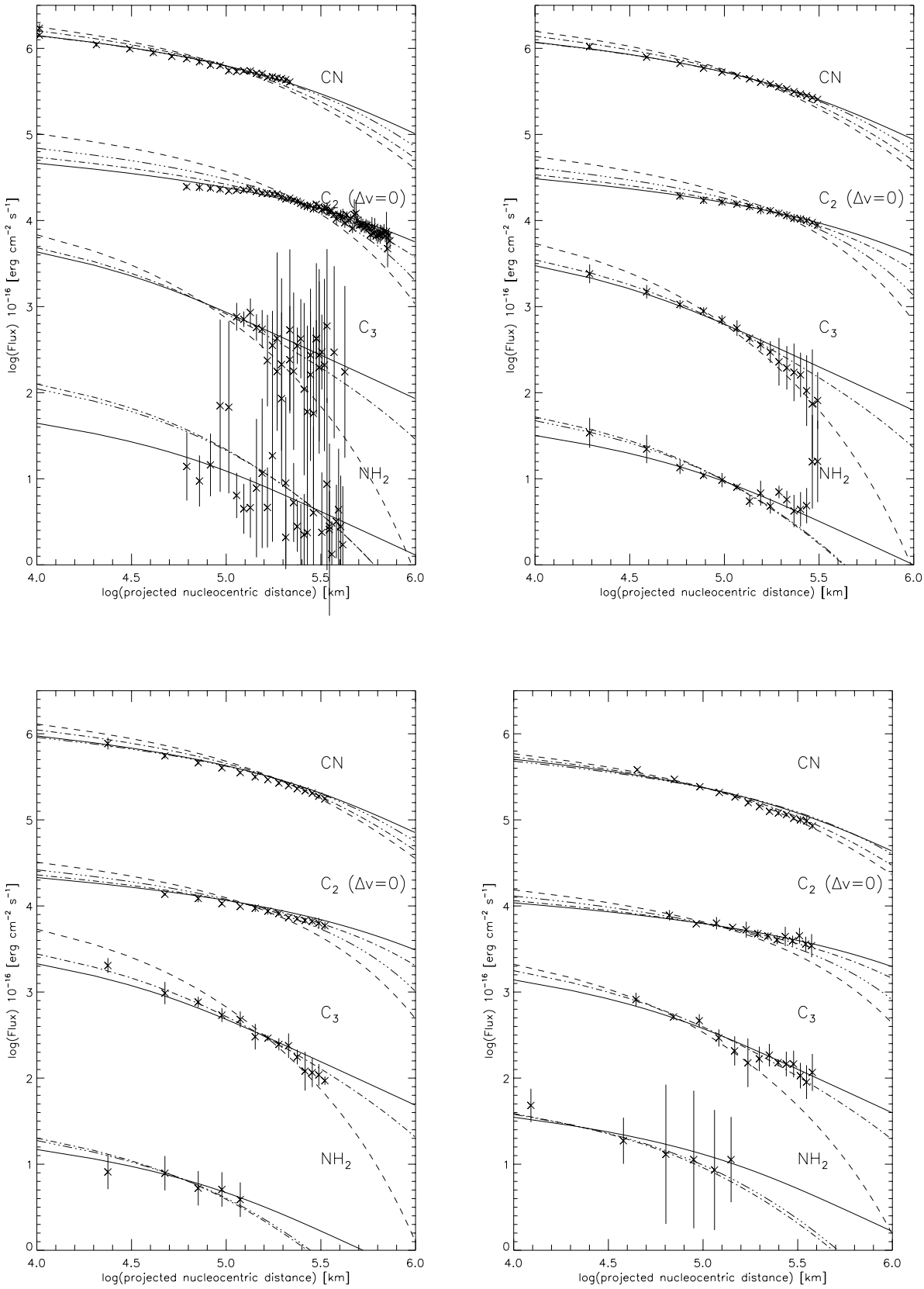

Figure 10.3: Radial profiles of CN, C_2, C_3 and NH_2 - top row from left to right: Dec. 6, 1997 at r_h=3.66 AU, Dec. 19, 1997 at r_h=3.78 AU, bottom row from left to right: Jan. 20, 1998 at 4.14 AU, Mar. 21, 1998 at 4.74 AU. Overplotted are the best fitting Haser profiles determined using different scale lengths. The measured profiles and the fitted Haser profiles of the radicals have been offset vertically for display.

$\mathbf{r}_h$ [AU]	**CN** [10^{25} s^{-1}]	$\mathbf{C_2}$ [10^{25} s^{-1}]	$\mathbf{C_3}$ [10^{25} s^{-1}]	$\mathbf{NH_2}$ [10^{25} s^{-1}]	**Date**
-4.60		44.4±13.6		22.2±0.1	25/26.04.1996
-4.60	20.0±0.1	23.6±0.1			26/27.04.1996
-3.98	35.8±5.4	46.3±3.0	1.7±0.6	8.5±0.1	24/25.06.1996
-3.98	64.6±13.8	58.4±12.0		36.7±5.6	25/26.06.1996
-3.34	78.7±33.1	47.9±19.1	9.1±2.1	6.2±0.2	19/20.08.1996
-3.34	79.9±0.1	56.5±14.3	9.2±0.1		18/19.08.1996
-3.34	124.9±24.1	98.9±20.8	11.6±0.1	60.3±19.9	23/24.08.1996
-3.10	197.1±25.3	141.4±21.6		102.5±12.9	13/14.09.1996
-2.85	183.8±64.6	203.6±29.1	27.2±10.2	59.6±1.1	02/03.10.1996
-2.85	190.4±42.8	183.3±40.7	33.8±10.0	86.4±36.2	03/04.10.1996
2.89	102.3±0.3	94.6±0.1		54.4±22.1	30/30.10.1997
3.63	29.5±0.3	28.9±7.8		14.4±3.5	07/08.12.1997
3.63	37.2±7.2	34.9±12.0	6.9±0.1	19.7±2.6	06/07.12.1997
3.78	26.0±4.7	24.1±5.9	4.7±0.9	15.4±2.2	19/20.12.1997
4.13	25.4±4.4	24.6±9.1	5.1±3.1		21/22.01.1998
4.13	29.8±6.8	27.9±5.9	6.7±3.1	9.5±0.9	20/21.01.1998
4.13	30.0±2.3	31.2±6.5	11.5±0.1		22/23.01.1998
4.74	18.9±2.3	14.5±6.8	7.1±6.4	2.2±0.6	17/18.03.1998
4.74	19.0±0.1	21.1±5.5	4.8±0.1	28.5±19.4	21/22.03.1998
6.00	4.9±1.3				06/07.08.1998
7.00	3.3±0.1				23/24.11.1998
7.00	4.4±1.1		≤0.63		24/25.11.1998
7.40	3.1±0.2				14/15.01.1999
7.40	3.7±1.1				13/14.01.1999
7.90	2.9±0.1				14/15.03.1999
9.80	0.86±0.15				12/13.11.1999
10.81	<1.8				05/06.04.2000
12.00	<0.16				29/30.09.2000
12.90	<0.06				20/21.01.2001
12.90	<0.05				24/25.01.2001

Table 10.4: Production rates computed using a Haser model. The Haser scale lengths used have been derived in this work (see Table 10.3).

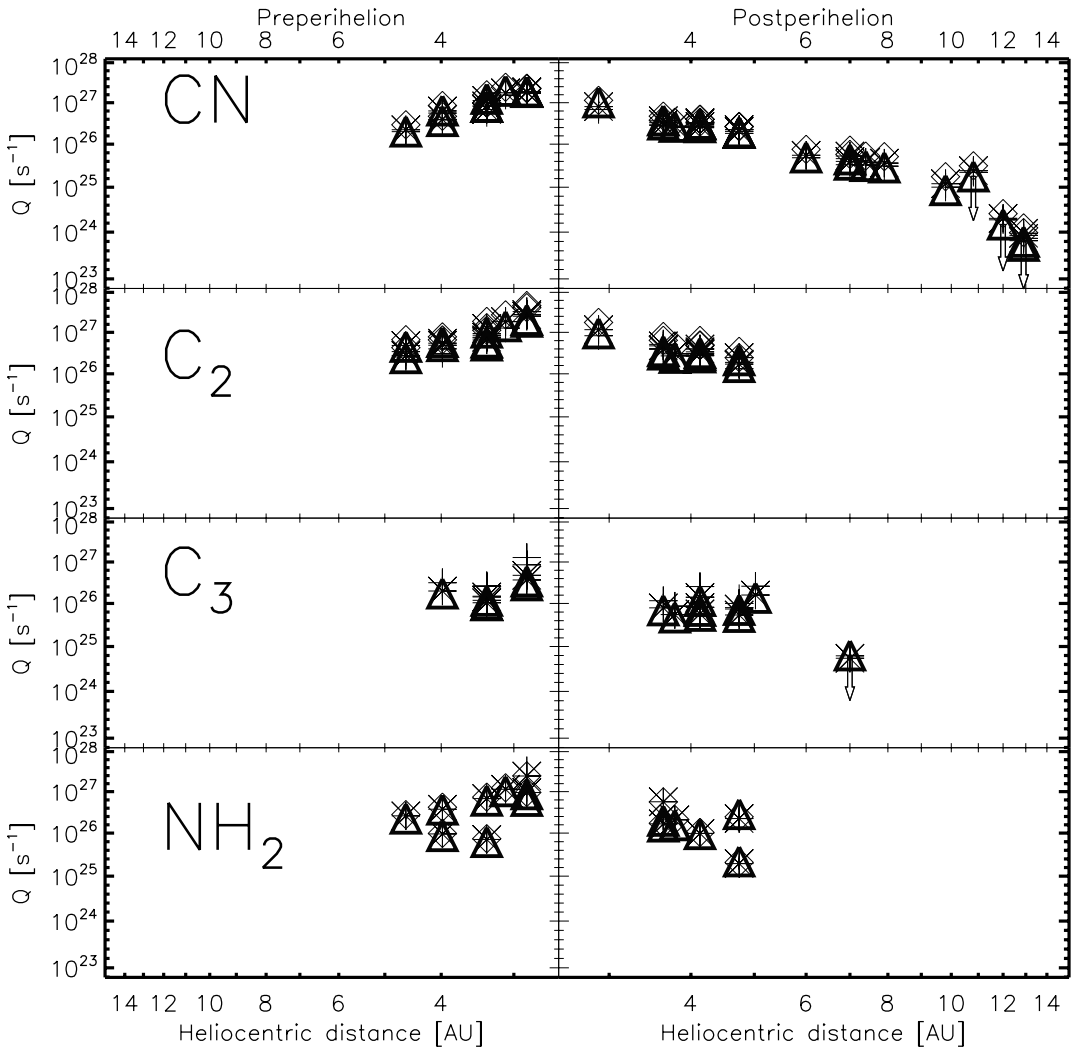

Figure 10.4: Production rates versus heliocentric distance computed using different Haser scale lengths taken from: crosses: A'Hearn *et al.* [1995]; stars: Cochran *et al.* [1992]; diamonds: Fink *et al.* [1991]; triangles: this work (see Table 10.3).

As can be seen clearly from Figure 10.4 the production rates derived using the different set of Haser scale lengths (see Table 10.3) show little differences. The differences have been quantified by the ratio

$$R = \frac{Q_{\mathrm{x}}}{Q_{\mathrm{this\ work}}} \tag{10.6}$$

where Q_{x} is the production rate determined with the Haser scale lengths given by A'Hearn *et al.* [1995], Cochran *et al.* [1992] and Fink *et al.* [1991], respectively. $Q_{\mathrm{this\ work}}$ is the production rate derived using the Haser scale length determined in this work. Table 10.5 gives the mean and in brackets the maximum ratio for each species and each set of Haser scale lengths used.

Molecule	A'Hearn	Cochran	Fink
CN	1.01 (1.37)	1.12 (1.52)	1.47 (2.02)
C_2	1.13 (1.78)	1.23 (1.36)	1.91 (2.34)
C_3	1.86 (2.31)	1.16 (1.39)	-
NH_2	-	1.34 (1.59)	1.40 (1.63)

Table 10.5: The mean and maximum (in brackets) ratios for the production rates computed with the Haser scale lengths given by different authors (see Table 10.3).

The derived production rates differ for most cases by far less than a factor of 2. Different scaling laws for the evolution with heliocentric distance used for the Haser scale lengths can create a trend over heliocentric distance. However, the effect is only significant if a wide range of heliocentric distances is covered. In this work CN production rates have been determined from 2.89 – 12.9 AU and the data is used to study possible trends with heliocentric distance computing the production rates with different Haser parent scale lengths. Figure 10.5 shows the results. Each panel displays the ratio R as defined in equation (10.6) for a set of Haser scale lengths published in the literature versus heliocentric distance. The ratio R only shows a slight increase with heliocentric distance. Most prominent is the trend for the scale lengths given by Fink resulting in a maximum ratio of $R = 2.02$ at 12.90 AU.
In summary, the effect of the different Haser scale lengths on the derived production rates is small. This means that production rates derived by different observers are still comparable even if slightly different sets of Haser scale lengths have been used. However, care should be taken if ratios of production rates are discussed.

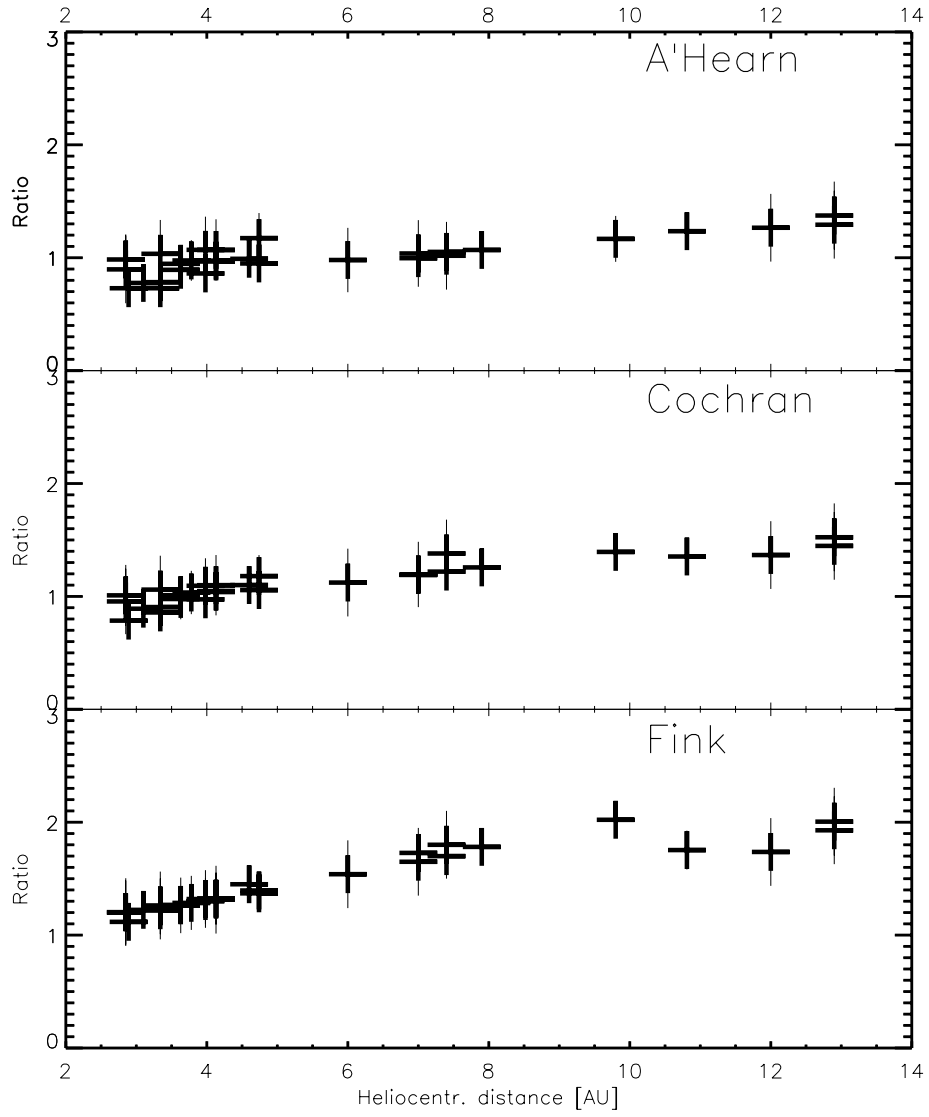

Figure 10.5: Ratio of the CN production rates determined using the Haser scale lengths from A'Hearn, Cochran, Fink (top to bottom) to the the CN production rates obtained using the Haser scale length determined in this work versus heliocentric distance.

10.5 Classification of comet Hale-Bopp in the taxonomy of comets

In order to study the variation in composition from one comet to another A'Hearn *et al.* [1995] introduced a classification scheme based on the ratio of production rates. The ratios have been calculated relative to CN and to OH production rate. The comet taxometry was based on the optical observation of a large number of comets. Most comets showed good agreement in the production rate ratios. They define the class of 'normal' comets. However, a small number of comets showed deviating production rate ratios. Most obvious was this effect for the $Q(C_2)/Q(CN)$ ratio, leading to the introduction of a class of so-called 'carbon-depleted' comets. For all production rate ratios A'Hearn *et al.* [1995] derived 'normal' values and values for 'depleted' comets.

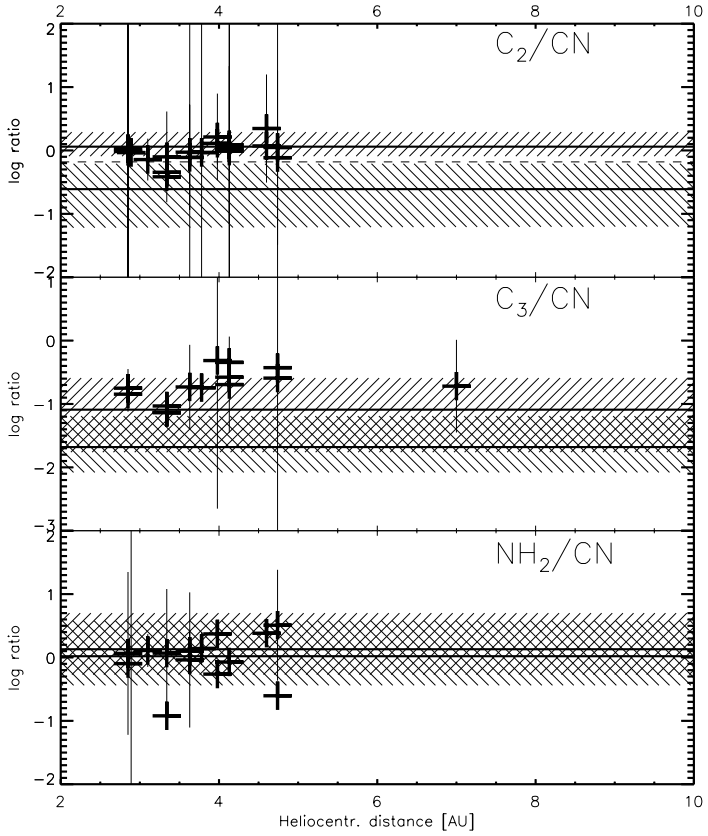

Figure 10.6: Ratio of C_2, C_3 and NH_2 production rates to CN production rate versus heliocentric distance computed using the Haser scale lengths derived in this work (see Table 10.3). Solid lines denote the mean value as given by A'Hearn *et al.* [1995] for 'typical' and 'depleted' comets. The range given for both classes is indicated as right hatches ('typical') and left hatches (depleted) [Rauer *et al.*, 2002].

In order to place comet Hale-Bopp in the framework of this taxometry, the ratio of the production rates of C_2, C_3, and NH_2 relative to CN have been computed. The production rates have been determined using the Haser scale lengths derived in this work. The logarithm of ratios are plotted versus heliocentric distance in Figure 10.6 in comparison to the classification given by A'Hearn. Using the same type of plot as in A'Hearn *et al.* [1995] allows an easy comparison.
The $Q(C_2)/Q(CN)$ and $Q(C_3)/Q(CN)$ ratio classifies comet Hale-Bopp as a normal comet. Furthermore no significant variation with heliocentric distance is found.
A'Hearn found in his study little differences in the Q(NH)/Q(CN) ratio among comets. The observations used in this work do not yield NH production rates. Based on the photochemistry of NH_2 (see section 5.4) NH is the direct dissociation product. Therefore, the ratio of $Q(NH_2)/Q(CN)$ is comparable to the ratio of Q(NH)/Q(CN). Figure 10.6 shows that for comet Hale-Bopp this ratio is in the range of a 'normal' comet. For more details see Rauer *et al.* [2002].
The comparison with the results by A'Hearn is slightly inconsistent, because the production rates have been determined using a different set of Haser scale lengths. It has already been discussed that the influence of the Haser scale length on the derived production rate is small. Therefore, the resulting effect on the ratios should be small as well. In Figure 10.7 the ratio $Q(C_2)/Q(CN)$ is plotted versus heliocentric distance again, but this time the production rates are derived using the Haser scale lengths given by A'Hearn. Comparing this to the top panel in Figure 10.6 shows no significant difference.

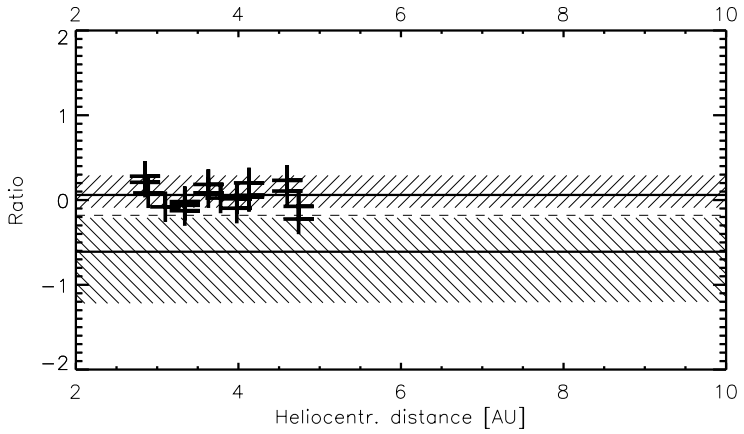

Figure 10.7: Ratio of $Q(C_2)/Q(CN)$ for production rates derived using the scale lengths given by A'Hearn *et al.* [1995] (Table 10.3)

10.6 Results from the Haser model analysis

The observational data collected during the Hale-Bopp monitoring program has been analyzed using the Haser model. For the first time effective Haser scale lengths have been determined directly for a comet at a heliocentric distance greater than 3 AU (Table 10.3). Using these Haser scale lengths production rates for all observed species have been derived. For NH_2 the derived Haser scale lengths and their evolution with heliocentric distance indicate strongly a formation in a single step process from a single parent. The results are consistent with the formation from NH_3 as parent molecule.
For CN the derived Haser scale lengths and their evolution with heliocentric distance indicate a formation in a single step process from a single parent, assuming that the daughter product receives some excess energy in the dissociation process. This is consistent with the formation from HCN as the dominant parent molecule. As shown in Rauer *et al.* [2002] a comparison of the CN production rate with the HCN production rate as measured by Biver *et al.* [1997] strongly supports this connection (see also Rauer *et al.* [1997]). For a more detailed discussion on CN and its parents see Rauer *et al.* [2002].
For C_2 and C_3 the evolution of Haser scale lengths with heliocentric distance clearly rule out the formation in a single photodissociation step from a single parent molecule. This is in agreement with the findings discussed in section 11.1 and 11.2. To understand the formation of these two radicals a more complex model than the Haser model is needed. Since the basic assumptions of the Haser model are violated, the production derived need to be treated with caution. They are still useful to compare with other results also obtained using the Haser model. The taxonomy by A'Hearn *et al.* [1995] is an example for this. Based on the Haser production rates comet Hale-Bopp is a 'normal' comet.